Deletion of DnaK's Lid Strengthens Binding to the Nucleotide Exchange Factor, GrpE: A Kinetic and Thermodynamic Analysis†

Liudmila S. Chesnokova,‡ Sergey V. Slepenkov,‡ Irina I. Protasevich,§ Michael G. Sehorn,‡ Christie G. Brouillette,§ and Stephan N. Witt*,‡

Department of Biochemistry and Molecular Biology, Louisiana State University Health Sciences Center, 1501 Kings Highway, Shreveport, Louisiana 71130-3932, and Biomolecular Analysis Group, Center for Biophysical Science and Engineering, University of Alabama at Birmingham, 1025 18th Street South, Birmingham, Alabama 35294

Received April 25, 2003; Revised Manuscript Received June 9, 2003

ABSTRACT: In this study, we have used surface plasmon resonance (SPR) and isothermal microtitration calorimetry (ITC) to study the mechanism of complex formation between the Hsp70 molecular chaperone, DnaK, and its cochaperone, GrpE, which is a nucleotide exchange factor. Experiments were geared toward understanding the influence of DnaK's three domains, the ATPase (residues 1−388), substrate-binding (residues 393−507), and lid (residues 508−638) domains, on complex formation with GrpE. We show that the equilibrium dissociation constants for the interaction of GrpE with wtDnaK, lidless DnaK(2−517), the ATPase domain (2−388), and the substrate-binding fragment (393−507) are 64 (±16) nM, 4.0 (±1.5) nM, 35 (±10) nM, and 67 (±11) μM, respectively, and that the on-rate constant for the different reactions varies by over 4 orders of magnitude. SPR experiments revealed that GrpE−DnaK(393−507) complex formation is inhibited by added peptide and abolished when the 33-residue flexible "tail" of GrpE is deleted. Such results strongly suggest that the 33-residue flexible N-terminal tail of GrpE binds in the substrate-binding pocket of DnaK. This unique mode of binding between GrpE's tail and DnaK contributes to, but does not fully explain, the decrease in K_d from 64 to 4 nM upon deletion of DnaK's lid. The possibility that deletion of DnaK's lid creates a more symmetrically shaped molecule, with enhanced affinity to GrpE, is also discussed. Our results reveal a complex set of molecular interactions between DnaK and its cochaperone GrpE. We discuss the impact of each domain on complex formation and dissociation.

The *Escherichia coli* Hsp70 chaperone DnaK functions cotranslationally and posttranslationally to promote protein folding and disaggregation in the cell. DnaK's reaction cycle is fueled by the binding and hydrolysis of ATP and is regulated by the two cochaperones, DnaJ and GrpE (*1*−*4*). DnaK shuttles between an ATP-bound form, which has low affinity for peptide substrates, and an ADP-bound form, which has relatively high affinity for protein substrates. DnaJ promotes substrate binding to the ATP-bound state and also stimulates ATP hydrolysis. The nucleotide exchange factor GrpE promotes ADP dissociation (*5*). Substrate ejection occurs in concert with ATP binding. The DnaK/DnaJ/GrpE reaction cycle, defined by repeated substrate binding and release, coupled to DnaK-mediated ATP hydrolysis, probably produces a conformational change in the substrate protein that increases the probability of proper folding (*4*). The mechanism by which DnaK transduces free energy from ATP binding and hydrolysis to conduct physical work on its substrates is unknown.

The GrpE protein was thought to be only expressed by bacteria. This turns out not to be the case. Several recent genetic studies have revealed that GrpE homologues are expressed in eukaryotic cells and are localized to the cytosol and the mitochondrion where they facilitate the import of cytosolic proteins into the mitochondrial matrix (*6*−*10*). The yeast homologue of the DnaK/DnaJ/GrpE chaperone machine is mtHsp70/Ydj1p/Mge1p. The cytosolic Hsp70 chaperones of yeast utilize a nucleotide exchange factor (*11*) that is distinct from Mge1p.

GrpE is a homodimer (*12*, *13*) that consists of three domains: paired N-terminal α-helices, four-helix bundles, and the C-terminal β-domains comprise residues 40−88, 89−137, and 139−197, respectively. Residues 1−33 are thought to exist in a disordered, flexible state. An X-ray crystallographic study revealed that the GrpE homodimer binds asymmetrically to the ATPase domain of DnaK (*14*): the proximal GrpE molecule, through its C-terminal β-domain, binds to lobes of the ATPase domain of DnaK (Figure 1A), and almost no contacts are made between the distal GrpE molecule and the ATPase domain. The two N-terminal parallel α-helices of GrpE appear to extend out far enough to interact with the C-terminal substrate-binding domain of DnaK (residues 393−507), which is absent in the crystal structure.

Several studies have shown that GrpE is probably more than just a nucleotide exchange factor; it is also involved in substrate release. One study showed that GrpE reduces the affinity of added peptides for the ATP-bound state of wtDnaK (*15*). Another study (*14*) showed that increasing

† Support for this work came from the NIH (GM51521) (S.N.W.).
* To whom correspondence should be addressed. Tel: (318) 675-7891. Fax: (318) 675-5180. E-mail: switt1@lsuhsc.edu.
‡ Louisiana State University Health Sciences Center.
§ University of Alabama at Birmingham.

10.1021/bi0346493 CCC: $25.00
Published on Web 07/12/2003

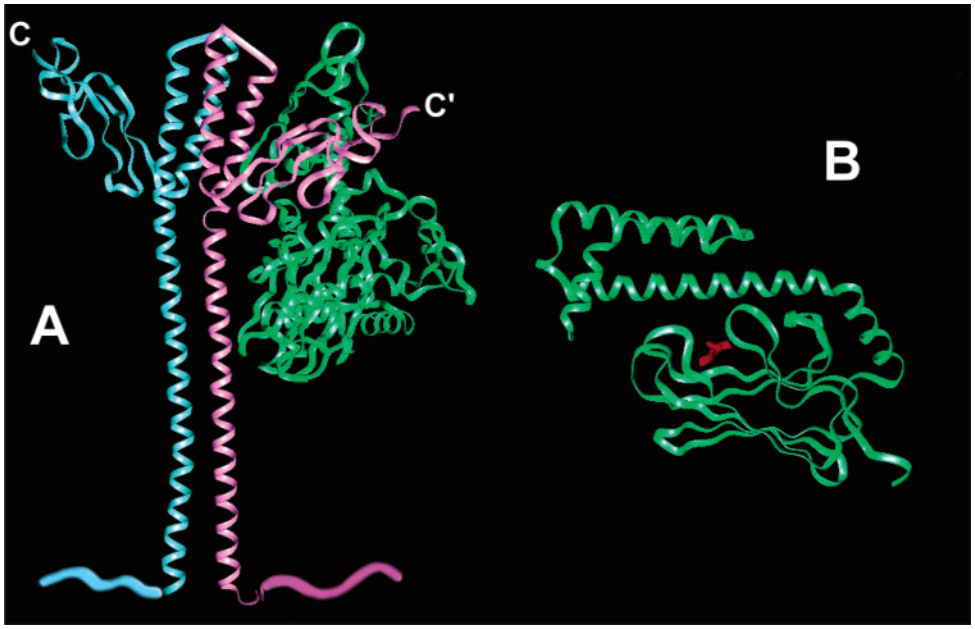

FIGURE 1: Structures of the GrpE and DnaK. (A) Structure of the GrpE homodimer complexed to the ATPase domain of DnaK (PDB 1DKG) (*14*). The proximal and distal GrpE monomers are shown in purple and light blue, respectively. The ATPase domain is shown in green. In total, there are six contact areas between DnaK and GrpE. The main interaction points are between the proximal β-sheet domain of GrpE and domains IB and IIB of DnaK. The estimated interaction surface area between the two proteins is ~2800 Å^2, which includes nonpolar, polar, and salt bridge interactions. The 33-residue, N-terminal flexible tail, while depicted for each monomer, does not appear in the X-ray structure. (B) Structure of the C-terminal substrate-binding and lid domains of DnaK (PDB 1DKX) (*48*). DnaK is shown in green and the bound peptide in red.

concentrations of GrpE in solution result in decreasing concentrations of ADP·wtDnaK·RCMLA (reduced carboxymethylated lactalbumin) complexes at equilibrium, where RCMLA is a permanently unfolded form of lactalbumin. Significantly, a truncated variant of GrpE in which 33 residues are deleted from the N-terminal, α-helical tail does not affect the amount of RCMLA bound to wtDnaK. Thus, residues 1−33 are required for this effect. Two recent studies reported that GrpE and even the N-terminal "tail" of GrpE accelerate peptide release from wild-type DnaK (*16*, *17*).

We are interested in how GrpE controls the kinetics of the DnaK reaction cycle. Elucidating the kinetics of GrpE·DnaK interactions, and the factors that govern complex formation, are crucial to understanding the overall DnaK reaction cycle because without GrpE the DnaK reaction cycle comes to a halt. This is especially true because there are hints that the slow step in the reaction cycle may be the binding of GrpE to ADP-bound DnaK. Specifically, GrpE binds to ADP-bound DnaK with an unusually small on-rate constant of $\sim 1.5 \times 10^3$ M^{-1} s^{-1} (*14*). In addition, the emerging evidence that GrpE participates in substrate release (*14*, *16*, *17*) and is a thermosensor (*18*−*21*) underscores the importance of this cochaperone. This initial study was undertaken to determine how the three domains of DnaK, the ATPase, the β-sandwich, and lid domains, affect the kinetics of GrpE·DnaK complex formation.

MATERIALS AND METHODS

Protein and Reagents. Reagents were of the highest purity and were purchased from Sigma, unless stated otherwise. wtDnaK and DnaK(2−517) were isolated using ATP−agarose and ion-exchange chromatographies, as previously described (*22*, *23*). Nucleotide was removed from DnaK and DnaK(2−517) by either exhaustive dialysis (*23*) or the method of Gao et al. that employs AMP-PNP (*24*). Protein was stored in the HEPES[1] sample buffer containing 10% glycerol at −80 °C prior to use.

DnaK(1−388). The pMSK plasmid harboring the wild-type *dnaK* gene behind an IPTG-inducible promoter was a gift to us from Dr. Lila Gierasch (University of Massachusetts, Amherst). Using the QuikChange site-directed mutagenesis kit (Stratagene), a stop codon was introduced into the *dnaK* gene such that translation terminates at residue 388. The forward and reverse primers were 5′-CTG ACT GGT GAC GTA AAA TAA GTA CTG CTG CTG G-3′ and 5′-CCA GCA GCA GTA CTT ATT TTA CGT CAC CAG TCA G-3′, respectively. To ensure that a secondary mutation was not introduced during the PCR protocol, the gene encoding DnaK(1−388) was sequenced at the Iowa State University DNA Sequencing & Synthesis Facility. This variant of DnaK was expressed in the DnaK-deficient *E. coli* strain BB1553 (*25*) and then purified and made nucleotide-free using the same methods as for the wild-type protein.

DnaK(393−507). The plasmid pET15b, which contains the gene coding for the β-sandwich domain of DnaK (*26*), residues 393−507, was a gift from Dr. Lila Gierasch (University of Massachusetts, Amherst). To facilitate purification, DnaK(393−507) contains an N-terminal His_6 tag. This plasmid was transformed into *E. coli* BL21(DE3) pLysS competent cells by standard procedures. IPTG (1 mM) was used to induce the overexpression of the DnaK fragment.

[1] Abbreviations: HEPES, *N*-(2-hydroxyethyl)piperazine-*N*′-2-ethanesulfonic acid; ITC, isothermal titration calorimetry; p5, synthetic peptide CLLLSAPRR; SPR, surface plasmon resonance; TCEP, tris(2-carboxyethyl)phosphine hydrochloride; wt, wild type.

Cells were lysed using a French press, and DnaK(393−507) was purified from the crude extract using a Ni-NTA resin according to the manufacturer's instructions, followed by the ion-exchange chromatography on the ResourceQ column. The protein, which eluted in the flow-through fraction of the ResourceQ column, was dialyzed against HEPES buffer (25 mM HEPES, 50 mM KCl, 5 mM $MgCl_2$, and 5 mM 2-mercaptoethanol, pH 7) (6 × 4 L).

DnaK(386−562). The plasmid pQE30, which contains the gene coding for the β-sandwich domain plus partial lid (*27*), residues 386−562, was a gift from Dr. Eric Zuiderweg (University of Michigan, Ann Arbor). To facilitate purification, DnaK(386−562) contains an N-terminal His_6 tag. This plasmid was transformed into *E. coli* BL21 cells, and the protein was expressed after the IPTG (1 mM) induction. The fragment was purified by the same protocol as DnaK(393−507), except that the first step, the Ni-NTA column, was conducted under denaturing conditions (8 M urea). The second chromatographic step involved ion-exchange chromatography using a MonoQ resin. The fragment, which eluted in the flow-through, was dialyzed against HEPES buffer (25 mM HEPES, 50 mM KCl, 5 mM $MgCl_2$, and 5 mM 2-mercaptoethanol, pH 7) (6 × 4 L).

GrpE. The plasmid pET3a, which contains the gene for the GrpE protein, was a generous gift from Drs. Ulrich Hartl and Manajit Hayer-Hartl (Max Planck Institute for Biochemistry, Martinsreid, Germany). (DNA sequencing confirmed the presence of the wild-type *grpE* gene.) The plasmid was transformed into *E. coli* BL21(DE3) pLysS cells, and protein was expressed after induction with IPTG (0.4 mM). GrpE was isolated using a DnaK affinity column (*16*). The protein was eluted from the DnaK -affinity column using ATP, dialyzed for 4 days against 16−20 L of HEPES sample buffer to remove residual nucleotide, and stored in HEPES sample buffer with 10% glycerol at −80 °C prior to use.

GrpE(34−197) was prepared using elastase (Sigma, no. E0258), which specifically cleaves between residues 33 and 34 (*14*). Briefly, GrpE (1−2 mg/mL) was incubated with elastase ([elastase]/[GrpE] = 1/500) in 0.2 M Tris-HCl, pH 8.6, at room temperature for 22 h. After digestion, concentrated KCl was added to a final concentration of 50 mM. The digest (∼10 mL) was then injected onto a ResourceQ 15 anion-exchange column, equilibrated in buffer A (50 mM KCl/25 mM Tris-HCl/1 mM EDTA/5 mM 2-ME, pH 7.8), that was connected to an Amersham Pharmacia FPLC. A linear AB gradient (2% B/min), where buffer B was 500 mM KCl/25 mM Tris-HCl/1 mM EDTA/5 mM 2-ME, pH 7.8, at 1.0 mL/min yielded two fractions. Fraction 1, which eluted at 16−18% B, contained low molecular weight peptides, whereas fraction 2, which eluted at 19−22% B, contained GrpE(34−197). Mass spectral analysis of the protein in the second fraction was consistent with GrpE-(34−197). In addition, N-terminal sequence analysis (Macromolecular Structure Analysis Facility, University of Kentucky, Lexington) of the GrpE fragment revealed the sequence AEQVDPR, which corresponds to residues 34−40 of GrpE. Protein was exhaustively dialyzed for 4 days against 16−20 L of HEPES sample buffer to remove residual ATP and stored in HEPES sample buffer with 10% glycerol at −75 °C prior to use.

GrpE and GrpE(34−197) were biotinylated using EZ-link TFP-PEO-biotin (*N*-{3-[2-(2-{3-[5-(2-oxohexahydrothieno-[3,4-*d*]imidazol-4-yl)pentanoylamino]propoxy}ethoxy)ethoxy]-propyl}succinamic acid 2,3,5,6-tetrafluorophenyl ester) (Pierce) according to the manufacturer's instructions. The nucleotide exchange factor and TFP-PEO-biotin were added to 1 mL of the HEPES sample buffer to final concentrations of 90 and 900 μM, respectively, and the mixture was gently shaken for 1 h at room temperature and then placed on ice for 4 h. Unreacted biotin was removed by exhaustive dialysis for 2−3 days against the HEPES sample buffer. The amount of biotin incorporated was determined with the HABA ([2-(4′-hydroxyazobenzene)benzoic acid]−avidin) (immunopure) reagent according to the manufacturer's (Pierce) protocol. For GrpE and GrpE(34−197) the ratio biotin:protein value from 0.78 to 1.0 was achieved. On the basis of experiments conducted using high-performance size exclusion chromatography on GrpE and biotinylated GrpE, biotinylation did not disrupt the GrpE dimer.

In this report, the symbol "−" represents a covalent bond, such as found between biotin and GrpE (biotin−GrpE), and "·" represents a noncovalent interaction, such as a complex between GrpE and wtDnaK (GrpE·wtDnaK). GrpE concentrations in the text refer to the GrpE dimer.

Surface Plasmon Resonance (SPR) Measurements. A BIACORE 2000 (Biacore AB) instrument was used to detect the formation of DnaK·GrpE complexes at the surface of the sensor chips. GrpE (or GrpE 34−197) was coupled to research grade CM5 sensor chips in a two-step procedure. Streptavidin was coupled to a sensor chip using the cross-linking reagent *N*-hydroxysuccinimide, *N*-ethyl-*N*′-(3-diethylaminopropyl)carbodiimide (Biacore), and then blocked with ethanolamine. This coupling procedure typically produced 4000 response units (RU) of signal. Biotinylated GrpE was then perfused over the chip and captured by the streptavidin molecules, yielding ∼400−600 RU. Each SPR experiment used multichannel detection: Flow cell 1 consisted of immobilized streptavidin saturated with biotin; flow cells 2 and 3 consisted of immobilized streptavidin with bound biotinylated GrpE; flow cell 4 consisted of the CM-dextran surface. Upon injection, DnaK was perfused simultaneously over each flow cell. The sensorgrams in this report represent the experimental sensorgram (flow cell 2 or 3) minus the control sensorgram (flow cell 1).

Frozen aliquots of DnaK (wild type or its variants) were thawed and centrifuged to remove aggregates, and protein concentration was then determined using the Bio-Rad reagent. Typically, an aliquot of concentrated DnaK was diluted into the running buffer. The running buffer in the Biacore experiments was 25 mM HEPES, 50 mM KCl, 5 mM $MgCl_2$, 5 mM 2-ME, and 0.005% Tween 20, pH 7.0. Flow rates were typically 40 μL/min. The sample buffer also contained 1 mg/mL CM-dextran (Fluka). The dextran reduces nonspecific interactions between the protein and the sensor chip. For DnaK(393−507), which is more hydrophobic than the other variants, 5 mg/mL CM-dextran and 0.025% sufactant P20 (Biacore, Inc.) were used.

All of the reactions analyzed here were conducted under pseudo-first-order conditions, viz., [DnaK] ≫ [GrpE]. Each sensorgram represents specific binding data minus the appropriate control. BIAevaluation software was used to zero the data. We found that the three truncated forms of DnaK (DnaK[2−517], DnaK[2−388], and DnaK[393−507]) bind to GrpE according to a 1:1 Langmuir interaction (eq 1). A

$$\text{DnaK} + \text{GrpE} \underset{k_{off}}{\overset{k_{on}}{\rightleftharpoons}} \text{DnaK·GrpE} \quad (1)$$

sensorgram of the above reaction consisted of an increase in signal, upon perfusing the analyte (DnaK) over immobilized GrpE, followed by a decrease in signal, upon washing with buffer. The increasing signal, $S(t)$, in the formation phase of each sensorgram followed the equation

$$S(t) = \Delta S(1 - e^{-k_{obs}^{on} t}) \quad (2)$$

where k_{obs}^{on} and ΔS are the observed first-order rate constant and amplitude, respectively. Values for k_{on} and k_{off} were obtained for the reaction of interest from the slope and y-intercept of the plot of k_{obs}^{on} versus [DnaK] (eq 3).

$$k_{obs}^{on} = k_{on}[\text{DnaK}] + k_{off} \quad (3)$$

Alternatively, on- and off-rate constants were obtained using BIAevaluation 3.0 software to simultaneously fit sensorgrams obtained from injections of three to eight different concentrations of analyte. Both methods gave the same results.

In contrast to the various truncated forms of DnaK, the wild-type protein reacts with GrpE in two discrete phases. The formation portion of the sensorgrams was fit to the equation

$$S(t) = S_1(1 - e^{-k_{obs,1}^{on} t}) + S_2(1 - e^{-k_{obs,2}^{on} t}) \quad (4)$$

where $k_{obs,1}^{on}$ and S_1 are the observed first-order rate constant and amplitude for the rapid phase, respectively, and $k_{obs,2}^{on}$ and S_2 are the observed first-order rate constant and amplitude for the slow phase, respectively. Explanations for the biexponential kinetics are given in the text.

Isothermal Titration Calorimetry (ITC) Measurements. A MicroCal, Inc., VP-ITC titration calorimeter was used to measure the thermodynamic parameters (K_d, ΔH, and ΔS) associated with the following two reactions: GrpE + wtDnaK ⇌ GrpE·wtDnaK and GrpE + DnaK(2−517) ⇌ GrpE·DnaK(2−517). For experiments on the wild-type protein, a solution of wtDnaK (4−10 μM) was loaded into the sample cell, and a solution of GrpE (34−90 μM dimer) was placed in the injection syringe. The first injection (1 μL) was followed by 20−40 injections of 7−14 μL. For experiments on DnaK(2−517), a solution of DnaK(2−517) (3.3−3.4 μM) was loaded into the sample cell, and a solution of GrpE (34−36 μM dimer) was placed in the injection syringe. The first injection (1 μL) was followed by 20 injections of 14 μL. Heats of GrpE dilution were measured by injecting the GrpE into the buffer solution and were subtracted from the experimental curves prior to data analysis. Data were analyzed according to Wiseman et al. (*28*) using version 5.0 of Origin (MicroCal, Inc.), assuming one set of sites. The protein solutions in the cell were stirred at 250 rpm, and the cell temperature was maintained at 25 °C (±0.02 °C). For the ITC experiments, GrpE and DnaK (wt or mutant) were contained in 25 mM HEPES, 50 mM KCl, 5 mM $MgCl_2$, and 2 mM TCEP at pH 7.0.

Stopped-Flow Fluorescence Measurements. A SX-18MV stopped-flow fluorescence spectrometer, Applied Photophysics Ltd. (Leatherhead, U.K.), was used to monitor ADP release from DnaK (*23*) with and without added GrpE. The instrument dead time was 1.3 ms, λ_{ex} = 295 nm (2.5 nm bandwidth), and fluorescence emission was collected at 90° to the incident light using an Oriel long-pass filter with cutoff wavelength of 320 or 335 nm. The instrumental time constant was equal to 0.5% of the half-time of the fastest phase. Samples were degassed prior to being loaded into the stopped-flow syringes. One syringe contained ADP·DnaK and the other Mg·ATP and GrpE. Temperature control of both the jacketed reactants and the jacketed mixing chamber was achieved with a circulating external water bath (ΔT = ±0.1 °C). Stopped-flow traces are the average of seven to ten individual traces.

Curve Fitting. The formation portion of the SPR sensorgrams was fitted to single- or double-exponential functions using a curve-fitting program that uses a Marquardt algorithm based on the program Curfit given in Bevington (*29*). The same software was used to fit the stopped-flow traces. Least-squares fitting of data to linear equations and determinations of standard errors of the fitted parameters were conducted using the program KaleidaGraph (Synergy Software, Reading, PA).

RESULTS

Wild-type DnaK consists of three domains: the ATPase domain, the β-sandwich domain, and the lid domain comprise residues 1−388, 393−507, and 508−638, respectively. The three-dimensional structures of the ATPase domain (bound to GrpE) and the β-sandwich and lid domains are shown in panels A and B of Figure 1, respectively. A schematic of the domain structure of wild-type DnaK and several variants used in this study is shown in Figure 2A. DnaK(2−517) comprises the ATPase and β-sandwich domains and one-half of the αA lid helix. DnaK(2−388) is the ATPase domain. DnaK(386−562) is the β-sandwich domain plus the αA and αB lid helices, and DnaK(393−507) is the β-sandwich domain. These proteins, visualized by SDS−PAGE with Coomassie blue staining, are shown in Figure 2B. GrpE-(34−197) was also used in this study; this protein is not shown on the gel.

NMR, as well as other biophysical techniques, has characterized the structure, dynamics, and folding behavior of the two substrate-binding domain fragments (*26*, *27*, *30*). The ATPase domain has been characterized by X-ray crystallography (*14*, *31*). On the basis of circular dichroism, size exclusion chromatography, and ANS binding experiments, we previously reported that DnaK(2−517) is a compact molecule that exhibits negligible self-association (*32*).

GrpE-Catalyzed ADP Dissociation from wtDnaK. Because biotinylated GrpE was used in our SPR experiments, it was necessary to test whether biotinylating GrpE alters its key function, which is to catalyze the release of ADP from ADP-bound DnaK. To this end, we measured the nucleotide exchange activity of labeled and unlabeled GrpE in the following fluorescence assay (*23*). A stopped-flow instrument was used to mix a volume of preformed ADP·DnaK complexes ([ADP] ≈ [DnaK]) with an equal volume of GrpE and excess ATP. Because ADP must dissociate before ATP binds (and quenches the tryptophan fluorescence of DnaK) and because ATP binding is fast, such experiments measure the rate of ADP dissociation from DnaK. However, the upper

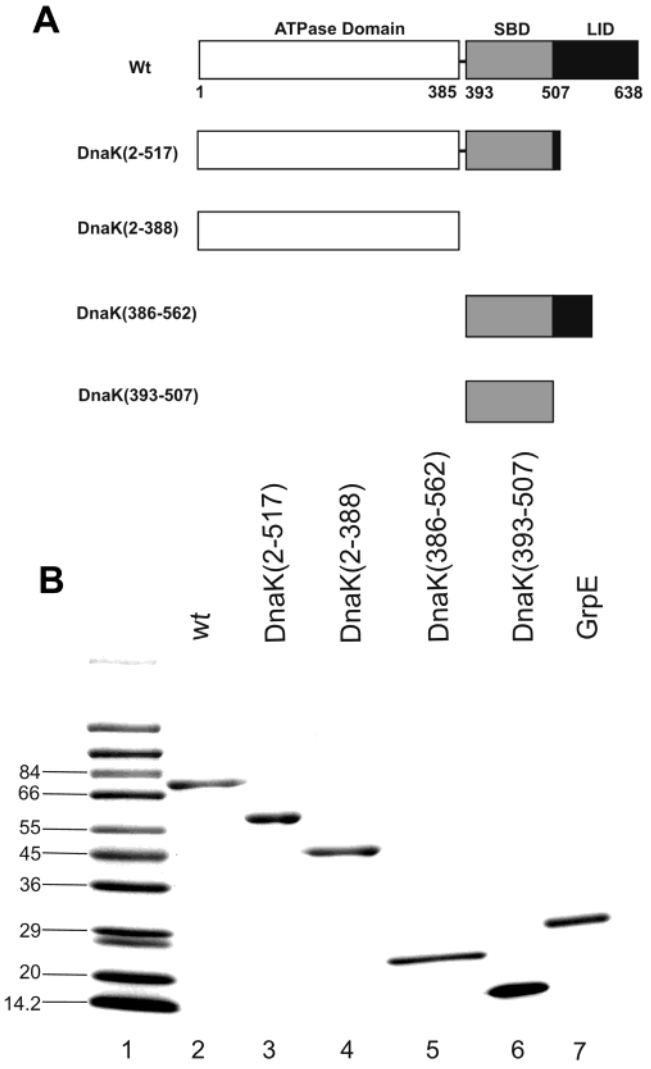

FIGURE 2: Domain structure (A) and SDS−PAGE analysis (B) of wtDnaK and its variants. Samples were analyzed using a discontinuous gradient gel (acrylamide: 7.5%/10%/12.5%) (*49*).

limit for the rate of ADP dissociation is the rate at which ATP binding quenches DnaK's tryptophan fluorescence.

Figure 3 compares uncatalyzed and catalyzed ADP dissociation from preformed ADP·wtDnaK complexes. In the absence of GrpE, and with zero added phosphate, ADP dissociates from wtDnaK in a single phase, with an apparent first-order rate constant of $0.022 \pm 0.002\ s^{-1}$ (trace 3), whereas, in the presence of GrpE, ADP dissociates from wtDnaK in two phases, with apparent first-order rate constants equal to $3.4 \pm 0.4\ s^{-1}$ ($k_{obs,1}$) and $0.39 \pm 0.04\ s^{-1}$ ($k_{obs,2}$) (trace 2). Identical values for these two constants are obtained when biotinylated GrpE is used instead of GrpE (trace 1). The experiments show that the biotinylation of GrpE does not alter its nucleotide exchange activity. We also determined that biotinylation of GrpE(34−197) does not alter its nucleotide exchange activity (data not shown).

DnaK·GrpE Complex Formation Probed by Surface Plasmon Resonance. The Biacore instrument employs a surface plasmon resonance technique to detect changes in the refractive index that occur upon binding of an analyte protein to its immobilized ligand. The change in the refractive index is proportional to the change in mass upon complexation.

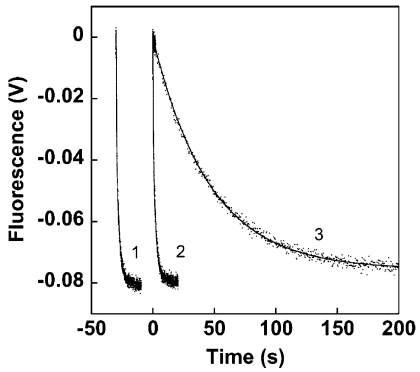

FIGURE 3: GrpE-catalyzed ADP dissociation from DnaK. Stopped-flow fluorescence experiments consisted of mixing [ADP·wtDnaK] with [GrpE + ATP], where brackets denote syringes. ADP dissociates from wtDnaK in two phases upon mixing with biotinylated GrpE ($k_{obs,1} = 3.4\ s^{-1}$ [40% amplitude] and $k_{obs,2} = 0.42\ s^{-1}$ [60% amplitude]) (trace 1), ADP also dissociates from wtDnaK in two phases upon mixing with GrpE ($k_{obs,1} = 4.0\ s^{-1}$ [40% amplitude] and $k_{obs,2} = 0.42\ s^{-1}$ [60% amplitude]) (trace 2), whereas ADP dissociates in a single phase in the absence of GrpE ($k_{obs} = 0.0217\ s^{-1}$) (trace 3). Reactant concentrations after mixing were 1 μM [DnaK·ADP], 2 μM GrpE, and 1.0 mM ATP. Because traces 1 and 2 are superimposable, trace 1 was offset to distinguish it from trace 2.

This technique is an ideal way to probe the kinetics of GrpE·DnaK interactions.

We found that immobilizing DnaK molecules on a CM5 sensor chip via amine coupling resulted in a significant reduction in the protein's ability to bind short peptides as well as GrpE. This loss of activity was also observed in a previous study (*33*). Thus, in the experiments described below, GrpE was immobilized on the sensor surface rather than DnaK. Specifically, biotinylated GrpE was immobilized on a sensor chip derivatized with streptavidin, and wtDnaK and its variants were perfused over the chip.

Herein, we focus on GrpE−DnaK interactions in the absence of ADP. The kinetics of GrpE·ADP·DnaK complex formation are considerably more complex than those involving the nucleotide-free chaperone. Because of this added complexity, we are in the process of devising a method whereby values for individual rate constants obtained from SPR experiments can be verified by a stopped-flow method. Results from that study will be reported at a later time. The analysis of how these individual domains of DnaK modulate the kinetics and thermodynamics of GrpE·DnaK complex formation is described below. All kinetic and thermodynamic experiments in this study were conducted at 25 °C.

GrpE + wtDnaK. Figure 4A shows sensorgrams for the reaction between GrpE and nucleotide-free wtDnaK. In addition to the kinetic experiments in which the concentration of wtDnaK was varied, two specificity controls were conducted: First, perfusing preformed ATP·wtDnaK complexes over GrpE results in no detectable complex formation. Second, perfusing ATP over the sensor chip during the dissociation phase results in a rapid loss of signal. Both results are consistent with an ATP-induced disruption of the GrpE·wtDnaK complex.

For the reaction between GrpE and nucleotide-free wtDnaK, the formation phase of each sensorgram was analyzed as follows. (i) Fits of the formation phases to a single exponential, and the respective residuals, are shown in Figure 4B,C. Overall, the fits are reasonable although they do not

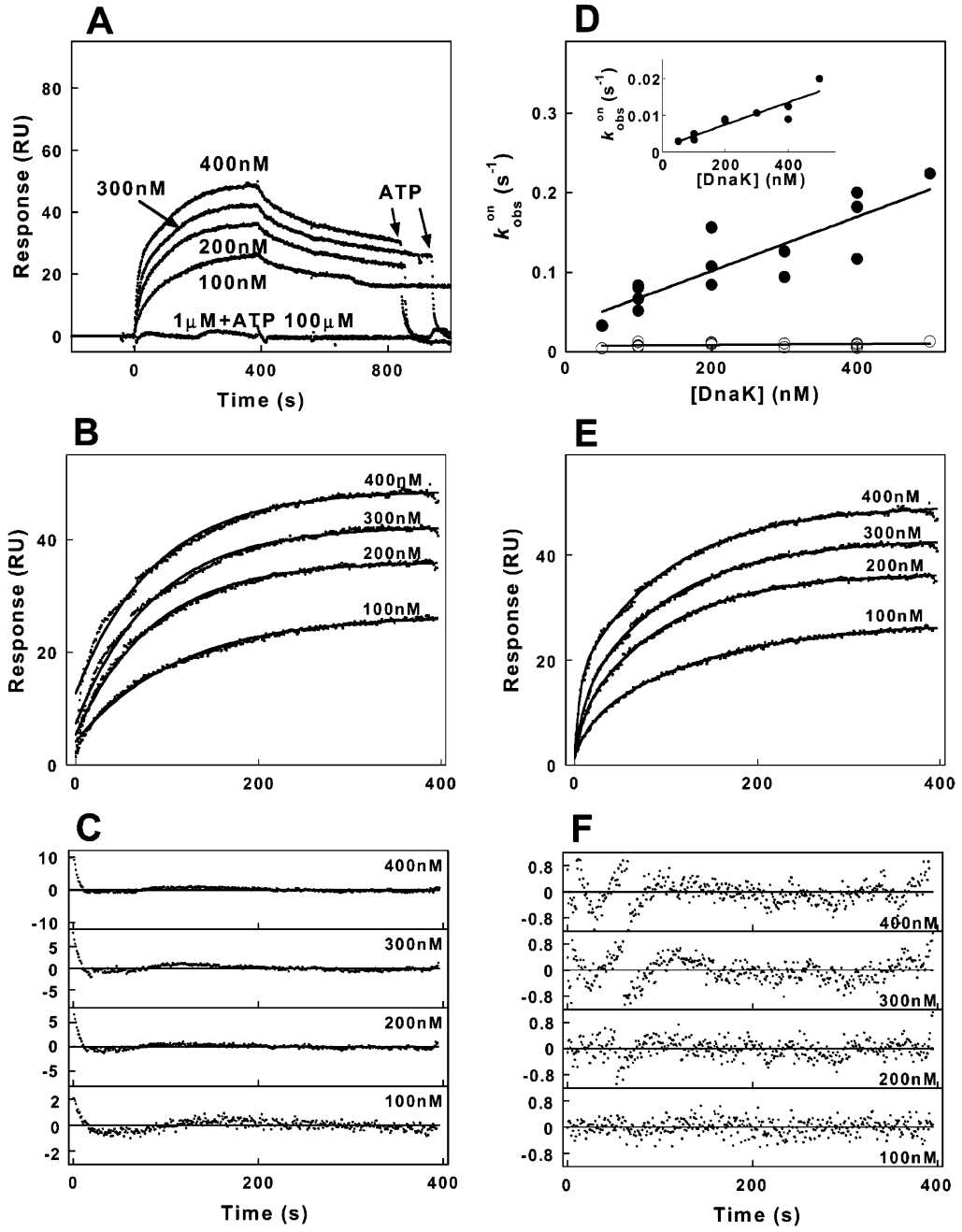

FIGURE 4: SPR analysis of the GrpE·wtDnaK interaction. (A) Sensorgrams for the reaction between wtDnaK and GrpE. In the control experiment, 100 μM ATP was preincubated with 1 μM wtDnaK for ~5 min and then perfused over GrpE. (B) The formation portion of each trace was fit to a single-exponential function (eq 2) (solid line), yielding values for k^{on}_{obs}. (C) Residuals for the single-exponential fits. (D) A plot of k^{on}_{obs} versus [wtDnaK] is shown in the inset to panel D. Values for k_{on} and k_{off}, determined from a linear least-squares fit of the data to a linear function (solid line), are $(3.0 \pm 0.5) \times 10^4$ M^{-1} s^{-1} and $(1.5 \pm 1.5) \times 10^{-3}$ s^{-1} ($R = 0.908$), respectively. (E) The formation portion of each trace was also fit to a double-exponential function (eq 4) (solid line), yielding values for $k^{on}_{obs,1}$ and $k^{on}_{obs,2}$. (F) Residuals for the double-exponential fits. (D) Plot of $k^{on}_{obs,1}$ versus [wtDnaK] (●). Values for k_{on} and k_{off}, determined from a linear least-squares fit of the data to a linear function (solid line), are $(3.4 \pm 0.6) \times 10^5$ M^{-1} s^{-1} and $(3.3 \pm 1.6) \times 10^{-2}$ s^{-1} ($R = 0.867$), respectively. The plot of $k^{on}_{obs,2}$ versus [wtDnaK] (○) is not well fit by a linear function ($R = 0.293$); the fit improves modestly when the data are fit to a hyperbolic function ($R = 0.4$). Data points in the plots of k_{obs} versus [wtDnaK] were obtained from experiments conducted on four different sensor chips. Temperature = 25 °C.

adequately mimic the early portions of the sensorgrams. Values for k^{on}_{obs} are plotted against [wtDnaK] (Figure 4D, inset), yielding k_{on} (slope) and k_{off} (y-intercept) values of $(3.0 \pm 0.5) \times 10^4$ M^{-1} s^{-1} and $(1.5 \pm 1.5) \times 10^{-3}$ s^{-1}, respectively. The value for k_{on} is quite similar to that previously reported by Harrison and co-workers for the reaction between nucleotide-free wtDnaK and immobilized GrpE ($k_{on} \approx 5 \times 10^4$ M^{-1} s^{-1} and $k_{off} \approx 1.5 \times 10^{-3}$ s^{-1}) (*14*). (ii) Fits of the formation phases to a double exponential, and the respective residuals, are shown in Figure 4E,F. The double-exponential fits capture much better the early portion ($t < 75$ s) of the sensorgrams. The amplitudes of the fast and slow phases are 39 ± 14% and 61 ± 13%, respectively. The plot of the observed first-order rate constant from the rapid phase, $k^{on}_{obs,1}$, versus [wtDnaK] is linear and yields k_{on} and k_{off} values of $(3.4 \pm 0.6) \times 10^5$ M^{-1} s^{-1} and (3.3 ± 1.6)

Table 1: Kinetic and Thermodynamic Constants for the Reaction between GrpE and Nucleotide-Free DnaK

	surface plasmon resonance			ITC
reaction	k_{on} (M^{-1} s^{-1})	k_{off} (s^{-1})	K_d (nM)	K_d (nM)[c]
DnaK + GrpE	$(3.0 \pm 0.5) \times 10^4$ [a]	$(1.5 \pm 1.5) \times 10^{-3}$ [a]	ND[d]	64 ± 16
	$(3.4 \pm 0.6) \times 10^5$ [b]	$(3.3 \pm 1.6) \times 10^{-2}$ [b]	97 ± 49[b]	
DnaK(2−517) + GrpE	$(2.7 \pm 0.2) \times 10^5$	$(1.2 \pm 0.2) \times 10^{-3}$	4.5 ± 1.5	3.5 ± 1.7
DnaK(2−388) + GrpE	$(1.3 \pm 0.1) \times 10^6$	$(4.6 \pm 1.3) \times 10^{-2}$	35 ± 10	ND
DnaK(393−507) + GrpE	$(1.0 \pm 0.1) \times 10^2$	$(6.7 \pm 0.6) \times 10^{-3}$	$(6.7 \pm 1.1) \times 10^4$	ND
DnaK(2−517) + GrpE(34−197)	$(1.30 \pm 0.05) \times 10^5$	$(2.7 \pm 0.4) \times 10^{-3}$	21 ± 7	ND

[a] Constants obtained from the fit to a 1:1 Langmuir model. [b] Constants obtained from the rapid phase of biexponential data (Figure 4D). [c] K_d values obtained with one set of binding sites. [d] ND, not determined.

$\times 10^{-2}$ s^{-1} ($K_d = 97$ nM), respectively (Figure 4D). On the other hand, the plot of $k^{on}_{obs,2}$ versus [wtDnaK] is not well fit by a linear function. Rate constants from analyses i and ii are given in Table 1. Our interpretation is that a rapid initial burst of complex formation occurs in the reaction between GrpE and nucleotide-free wtDnaK. Possible mechanisms, and the origin of the second phase of the reaction, are addressed in the Discussion.

GrpE + the Lidless DnaK Variant. The next reaction we investigated was the reaction between GrpE and the lidless variant, DnaK(2−517) (Figure 2A). Sensorgrams obtained over a range of DnaK(2−517) concentrations are shown in Figure 5A. As expected, increasing the concentration of DnaK(2−517) increases both the initial rate and the magnitude of the equilibrium end point. As a control, we found that, similar to the wild-type protein, perfusing preformed ATP·DnaK(2−517) complexes over immobilized GrpE results in no complex formation.

The formation portion of each trace was fit to both single- (Figure 5B) and double-exponential functions. Using a double-exponential function did not appreciably improve the residuals; thus we conclude that GrpE·DnaK(2−517) complex formation occurs according to a 1:1 Langmuir interaction. Values for k_{on} [$(2.7 \pm 0.2) \times 10^5$ M^{-1} s^{-1}] and k_{off} [$(1.2 \pm 0.2) \times 10^{-3}$ s^{-1}] were obtained from the plot of k^{on}_{obs} versus [DnaK(2−517)] (Figure 5A, inset). The equilibrium dissociation constant for GrpE binding to DnaK(2−517), calculated from these kinetic constants, is 4.3 ± 1.5 nM (Table 1). On the basis of this set of experiments, we conclude that deleting DnaK's lid (residues 518−638) increases the affinity of the DnaK·GrpE interaction by specifically slowing down complex dissociation [compare k_{off}(lidless) $(1.2 \pm 0.2) \times 10^{-3}$ s^{-1} to k_{off}(wt) $(3.3 \pm 1.6) \times 10^{-2}$ s^{-1}; Table 1].

Given the reports that the N-terminal flexible tail of GrpE promotes peptide release from DnaK (*14*−*17*), the above results indicate that deletion of DnaK's lid relieves steric hindrance of the substrate-binding pocket, which enables GrpE's tail to bind in the pocket. If the hypothesis that GrpE's tail binds in the substrate-binding site of DnaK is true, and if such binding retards GrpE·DnaK(2−517) complex dissociation, then we predict that (i) deleting the substrate-binding fragment from the lidless variant (DnaK517 → DnaK388) should increase the rate of complex dissociation [compared to the DnaK(2−517)·GrpE complex dissociation] and (ii) GrpE but not GrpE(34−197) should bind to the substrate-binding domain of DnaK. These hypotheses were tested below.

GrpE + the ATPase Domain of DnaK. Figure 6A,B shows sensorgrams for the reaction between GrpE and the ATPase domain of DnaK, DnaK(2−388). This domain is depicted schematically in Figures 1A and 2A. Inspection of the sensorgrams reveals that equilibrium (defined as no further change in signal) is achieved much faster for this reaction compared to the reactions involving the wild-type and lidless proteins (Figures 4 and 5). Such rapid equilibration indicates that k_{on} for this reaction is quite large. Also notice that because no change in refractive index occurs when preformed ATP·DnaK(2−388) complexes are perfused over immobilized GrpE, ATP disrupts GrpE·DnaK(2−388) complex formation. This means that ATP binding alters the conformation of the ATPase domain in such a way as to abolish binding to GrpE.

Fits of the formation phases to a single exponential, and the respective residuals, are shown in Figure 6B,C. On the basis of the fits, we reasonably conclude that GrpE and DnaK(2−388) interact according to a 1:1 Langmuir model. Values for k_{on} and k_{off} of $(1.2 \pm 0.1) \times 10^6$ M^{-1} s^{-1} and $(42 \pm 16) \times 10^{-3}$ s^{-1}, respectively, were obtained from the plot of k^{on}_{obs} versus [DnaK(2−388)] (Figure 6A, inset). The equilibrium dissociation constant for GrpE binding to DnaK(2−388), calculated from these kinetic constants, is 34 ± 13 nM (Table 1). Compared to DnaK(2−517), deletion of the substrate-binding domain has a dual effect: k_{on} and k_{off} increase ~5- and 38-fold, respectively (Table 1).

To assess whether the reaction between GrpE and DnaK(2−388) is affected by mass transport limitations, the following controls were conducted. Reducing the amount of immobilized biotinylated GrpE to approximately 30−70 RU/flow cell lowered the signal but did not significantly affect the magnitudes of the on- and off-rate constants. Additionally, the magnitudes of the rate constants were not affected by increasing the flow rate from 40 to 100 μL/min.

GrpE + the Substrate-Binding Fragment of DnaK. The ability of GrpE to bind to the substrate-binding domain of DnaK was tested. This variant, DnaK(393−507), is depicted schematically in Figure 2B. Figure 7A shows sensorgrams for the reaction between GrpE and the β-sandwich domain, DnaK(393−507). Unlike the other reactions, much higher concentrations of DnaK(393−507) had to be used (10−70 μM) to obtain a signal. This suggests that the interaction between DnaK(393−507) and GrpE is relatively weak; i.e., k_{on} is quite small or k_{off} is quite large or both. Indeed, assuming a 1:1 Langmuir interaction (Figure 7B,C), values for k_{on} and k_{off} values of $(1.0 \pm 0.14) \times 10^2$ M^{-1} s^{-1} and $(6.7 \pm 0.6) \times 10^{-3}$ s^{-1}, respectively, were determined from the plot of k^{on}_{obs} versus [DnaK(393−507)] (Figure 7A, inset). The equilibrium dissociation constant for GrpE binding to DnaK(393−507), calculated from these kinetic constants, is 67 ± 11 μM (Table 1). The experiments are the first to reveal

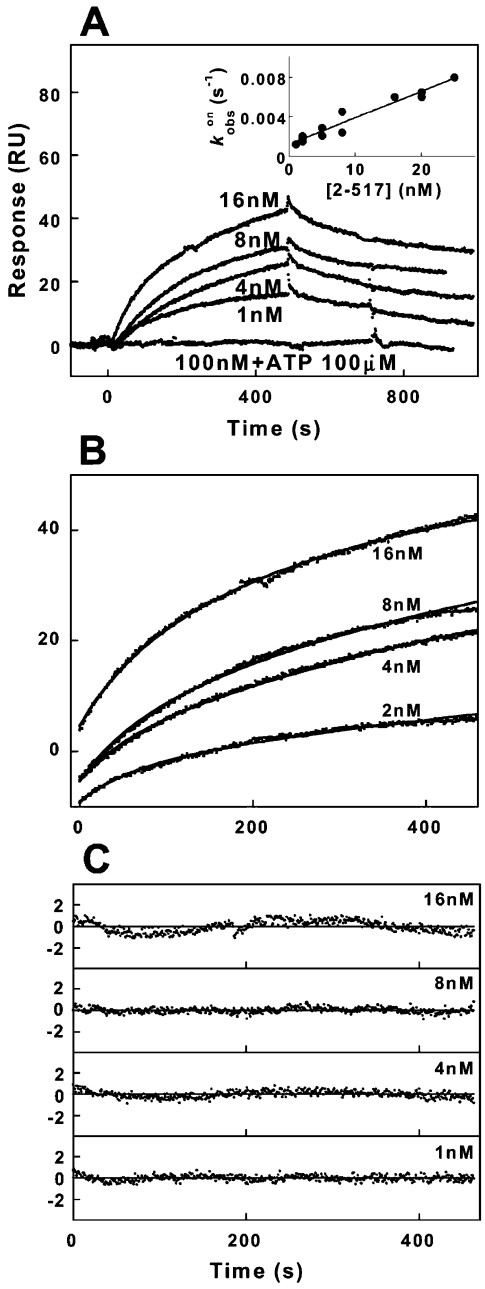

FIGURE 5: SPR analysis of the GrpE·DnaK(2−517) interaction. (A) Sensorgrams for the reaction between DnaK(2−517) and GrpE. In the control experiment, 100 μM ATP was preincubated with 0.1 μM DnaK(2−517) for ∼5 min and then perfused over GrpE. (B) The formation portion of each trace was fit to a single-exponential function (eq 2), yielding values for k_{obs}^{on}. Values for k_{on} and k_{off}, determined from a linear least-squares fit of the data (A, inset) to a linear function (solid line), are $(2.7 \pm 0.2) \times 10^5$ M^{-1} s^{-1} and $(1.2 \pm 0.2) \times 10^{-3}$ s^{-1} ($R = 0.972$), respectively. Data points in the plot were obtained from experiments conducted on three different sensor chips. (C) Residuals. Temperature = 25 °C.

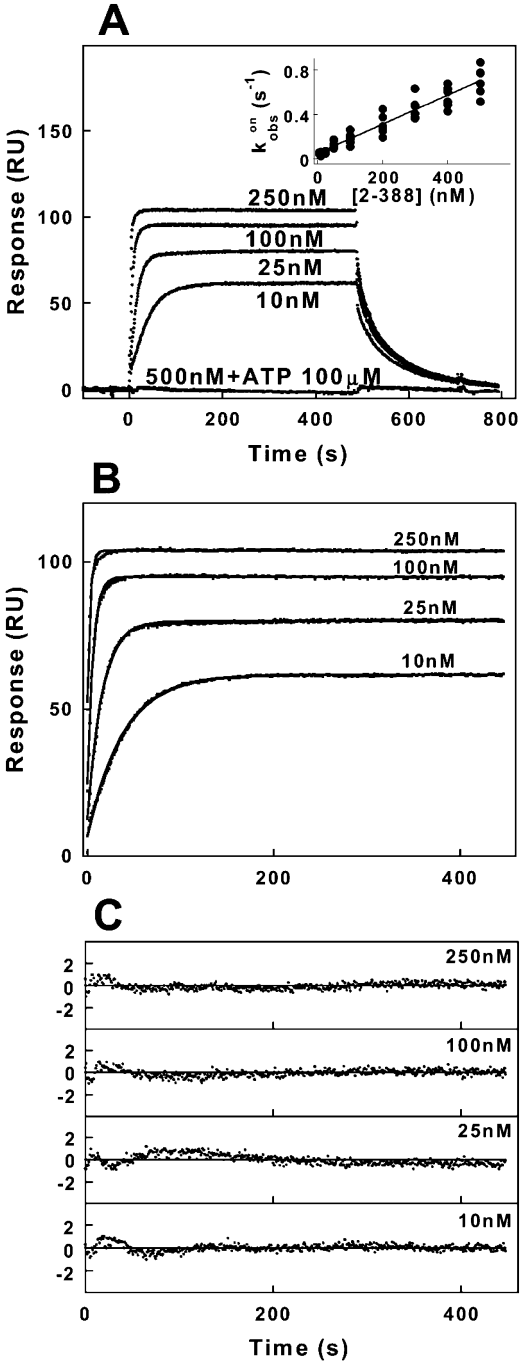

FIGURE 6: SPR analysis of the GrpE·DnaK(2−388) interaction. (A) Sensorgrams for the reaction between DnaK(2−388), the ATPase domain, and GrpE. In the control experiment, 100 μM ATP was preincubated with 0.5 μM DnaK(2−388) for ∼5 min and then perfused over GrpE. (B) The formation portion of each trace was fit to a single-exponential function (eq 2), yielding values for k_{obs}^{on}. Values for k_{on} and k_{off}, determined from a linear least-squares fit of the data (A, inset) to a linear function (solid line), are $(1.32 \pm 0.05) \times 10^6$ M^{-1} s^{-1} and $(4.6 \pm 1.3) \times 10^{-2}$ s^{-1} ($R = 0.957$), respectively. Data points in the plot were obtained from experiments conducted on three different sensor chips. (C) Residuals. Temperature = 25 °C.

that a weak binding interaction takes place between the substrate-binding domain and GrpE. The experiments described below hone in on whether the tail residues of GrpE are necessary for GrpE−DnaK(393−507) complex formation.

The hypothesis to be tested is that GrpE residues 1−33 bind, like a peptide, into the substrate-binding pocket of DnaK. (i) If this hypothesis is true, then added peptide should inhibit GrpE−DnaK(393−507) complex formation. SPR experiments were performed to test this idea; viz., DnaK(393−507) or DnaK(393−507)·p5 complexes were perfused over immobilized GrpE. (Ideally, complexes between DnaK(393−507) and GrpE(1−33) should be used in this experiment. We had the GrpE fragment 1−33 synthesized; however, the peptide has such poor solubility in the HEPES

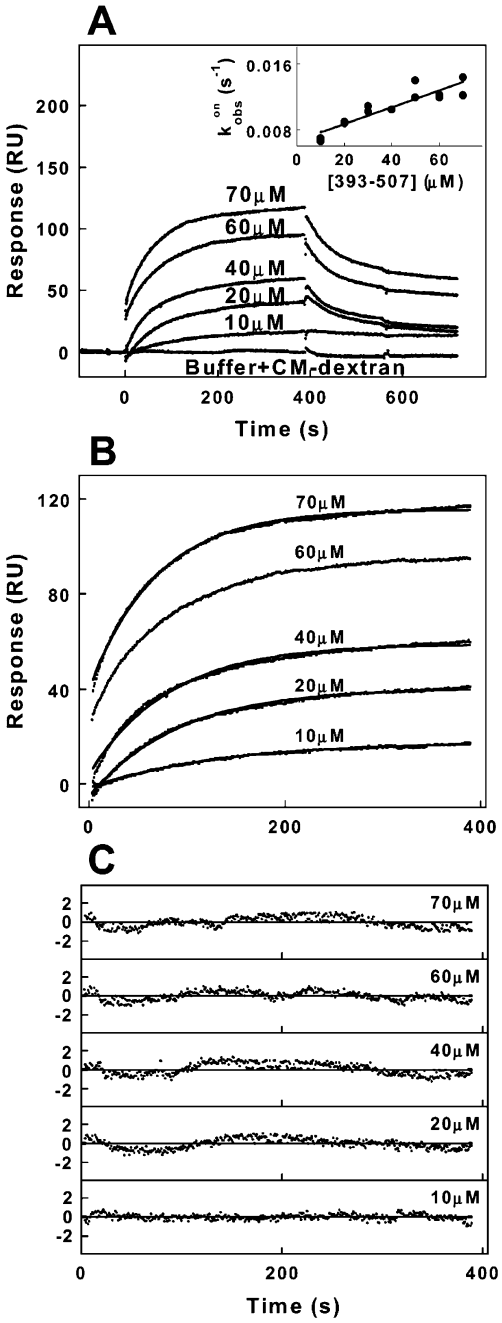

FIGURE 7: SPR analysis of the GrpE·DnaK(393−507) interaction. (A) Sensorgrams for the reaction between DnaK(393−507), the β-sandwich domain, and GrpE. (B) The formation portion of each trace was fit to a single-exponential function (eq 2), yielding values for k_{obs}^{on}. Values for k_{on} and k_{off}, determined from a linear least-squares fit of the data (A, inset) to a linear function (solid line), are $(1.0 \pm 0.1) \times 10^2$ M^{-1} s^{-1} and $(6.7 \pm 0.6) \times 10^{-3}$ s^{-1} (R = 0.908), respectively. Data points in the plot were obtained from experiments conducted on three different sensor chips. (C) Residuals. Temperature = 25 °C.

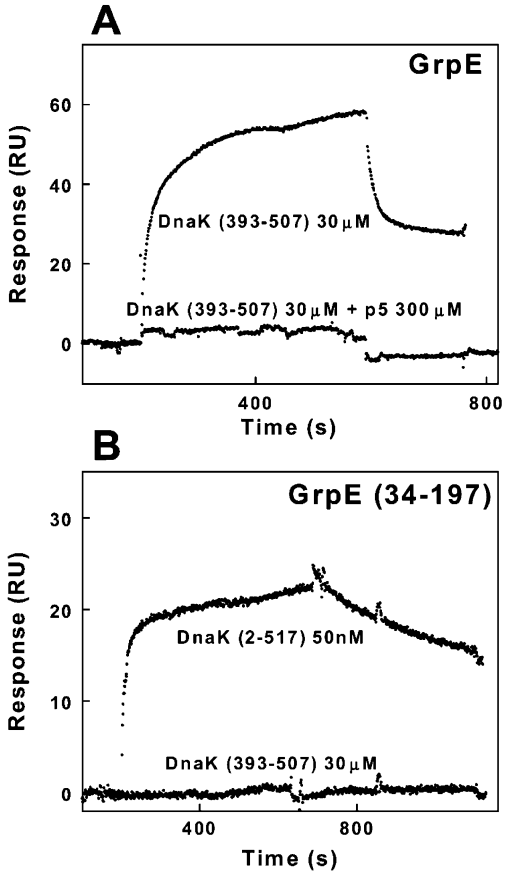

FIGURE 8: GrpE(1−33) binds to the substrate-binding domain of DnaK. (A) DnaK(393−507)·GrpE complex formation is inhibited by added peptide. Sensorgrams show the response as 30 μM wtDnaK or 30 μM wtDnaK·p5 complexes are perfused over immobilized GrpE. (B) DnaK(393−507) shows no binding to GrpE-(34−197). Sensorgrams show the response as 30 μM DnaK(393−507) or 50 nM DnaK(2−517) is perfused over immobilized GrpE(34−197). Kinetic constants for DnaK(2−517)·GrpE(34−197) complex formation are shown in Table 1. Temperature = 25 °C.

sample buffer that it is impossible to use it.) The results in Figure 8A illustrate that complex formation occurs when 30 μM DnaK(393−507) is perfused over GrpE. In contrast, complex formation is abolished when 30 μM DnaK(393−507)·p5 complexes are perfused over GrpE. (ii) SPR experiments were also conducted using DnaK(386−562), which is a fragment comprised of the β-sandwich peptide-binding domain and two lid helices (αA and αB) (Figure 2A). NMR experiments have shown that the B-helix of DnaK(386−562) is tightly bound within the peptide-binding domain of this fragment (*27*). It was expected that self-binding would inhibit complex formation between DnaK(386−562) and GrpE. Indeed, no signal was observed in the experiments in which DnaK(386−562), even at quite high concentration (100 μM), was perfused over immobilized GrpE (data not shown). This result agrees with a previous report showing that GrpE does not bind to the β-sandwich domain of DnaK that also contains the lid (*34*). (iii) If the 33 residues of the N-terminal tail of GrpE are a chaperone substrate, then GrpE(34−197), which lacks the tail residues, should not bind to DnaK(393−507). SPR experiments were conducted to test this idea. Indeed, perfusing 30 μM DnaK(393−507) over immobilized GrpE(34−197) results in no detectable complex formation (Figure 8B). A control experiment confirms that GrpE(34−197) is active: 50 nM DnaK(2−517) forms specific complexes with GrpE(34−197) (Table 1). The above experiments demonstrate that residues 1−33 of GrpE are essential for GrpE−DnaK(393−507) complex formation. The overall results suggest that residues 1−33 of GrpE act like a peptide substrate and bind in the substrate-binding pocket of DnaK-(393−507).

Isothermal Titration Calorimetry. To verify K_d values obtained from the SPR experiments, two of the reactions between GrpE and DnaK were also investigated by ITC.

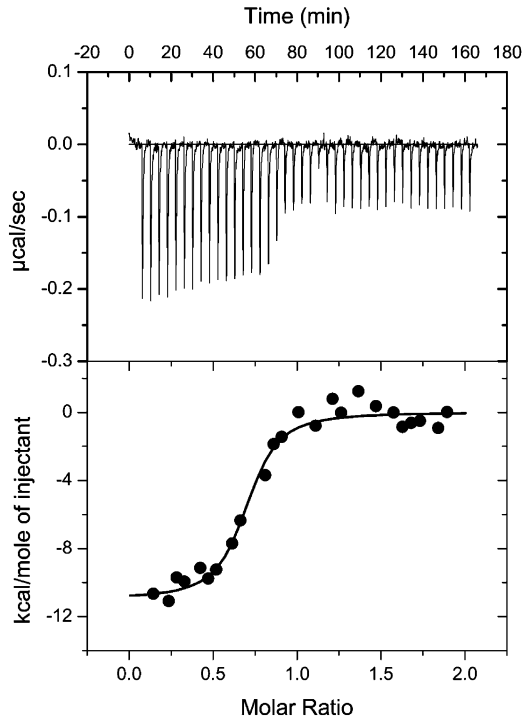

FIGURE 9: ITC data of the GrpE binding to wtDnaK at 25 °C in 25 mM HEPES, 50 mM KCl, 5 mM $MgCl_2$, and 2 mM TCEP, pH 7.0. Upper panel: heat released per second during the addition of 1×1 μL followed by 40×7 μL aliquots of the 45 μM GrpE dimer into the ITC cell containing 6 μM wtDnaK. Lower panel: integrated binding isotherm (circles, derived from upper panel) and experimental fit (solid line) to a single site model. The best fit parameters (from three experiments) are the equilibrium dissociation constant $K_d = 64 \pm 16$ nM, binding enthalpy $\Delta H = -12.3 \pm 0.9$ kcal/mol, and a molar binding stoichiometry of 1 GrpE dimer:1 wtDnaK (0.75 ± 0.04).

Figure 9 shows data for the titration of wtDnaK with the GrpE dimer. (The top panel shows the injection data, and the bottom panel shows the integrated data that is fit to one set of binding sites, i.e., a 1:1 interaction.) Heat is released upon adding GrpE, consistent with an exothermic reaction (top panel of Figure 9). From three different measurements, average values for the equilibrium dissociation constant, K_d, and stoichiometry of binding, N, are $K_d = 64 \pm 16$ nM and $N = 0.75 \pm 0.04$ (GrpE dimer per wtDnaK molecule). The average K_d is identical within the experimental error to the value determined from the SPR experiments ($K_d = 97 \pm 49$ nM; Table 1). The fitted stoichiometry of 0.75 deviates from the expected 1:1 stoichiometry, and the possible significance of this observation will be addressed in the Discussion.

For the titration of DnaK(2−517) with the GrpE dimer (data not shown), average values for K_d and N, from two different measurements, are 3.5 ± 1.7 nM and 1.00 ± 0.04 [GrpE dimer per DnaK(2−517) molecule], respectively. This average K_d value ($=3.5 \pm 1.7$ nM) is identical within the experimental error to the value determined from the SPR experiments ($K_d = 4.5 \pm 1.5$ nM; Table 1). Overall, the SPR and ITC experiments yield quite similar results.

We also report that when a dilute solution of DnaK (1 μM) is injected onto a high-performance size exclusion column, the DnaK monomer elutes with a molecular mass between 90 and 100 kDa. The observed mass of the DnaK monomer is greater than the theoretical mass of 69 kDa because DnaK is an asymmetrically shaped molecule (*35*). On the other hand, when an aliquot of DnaK(2−517) is injected onto the same column, the observed mass exactly equals its theoretical mass of 56 kDa (data not shown). These results suggest that the DnaK(2−517) is a more symmetric molecule than its wild-type counterpart.

DISCUSSION

Mechanism of the GrpE·wtDnaK Interaction. According to our surface plasmon resonance experiments, complex formation between GrpE and nucleotide-free wtDnaK deviates from a simple 1:1 Langmuir interaction. Sample heterogeneity often causes such a deviation (*35*). GrpE, for example, might exist in two conformations on the surface of the chip, or wtDnaK might exist in two conformations in solution, or both. On the other hand, if GrpE is heterogeneous, then we expect two phases of signal change in all of the reactions that we studied. But this was not the case.

Some feature of the wtDnaK protein must be responsible for the complex kinetics, because deviation from the 1:1 Langmuir model occurs only for the wild-type protein. Our view is that ligand-free wtDnaK is heterogeneous and this causes the deviation. Two mechanisms most likely to create heterogeneity are discussed. (i) The most obvious explanation is that wtDnaK self-associates (*12*); thus, our solutions of wtDnaK consist of monomers, dimers, and higher order species. On the other hand, several studies have shown that no detectable dimerization occurs at wtDnaK concentrations at or below 0.1 mg/mL (*12*). Because wtDnaK concentrations (0.0035−0.035 mg/mL) far less than 0.1 mg/mL were used in this study, it is most likely that the concentrations of dimers and higher order wtDnaK species are vanishingly small. For this reason, aggregation is reasonably ruled out as the cause of the deviation from a 1:1 Langmuir interaction. (ii) We have evidence that low concentrations (0.1−2 μM) of nucleotide- and peptide-free wtDnaK, while monomeric, are conformationally heterogeneous and that the heterogeneity is linked to the presence of the C-terminal residues 596−638 (*36*). Our interpretation is that the conformational heterogeneity of the wild-type protein is abolished by deleting residues 518−638, and this is why DnaK(2−517)·GrpE complex formation obeys a 1:1 Langmuir interaction.

Both SPR experiments and ITC experiments show a deviation from the expected 1:1 interaction between GrpE and wtDnaK. The most likely explanation for the ITC experiments is related to the reported self-association of wtDnaK (*12*). That study has shown that no detectable dimerization occurs at wtDnaK concentrations lower than 0.1 mg/mL. In the ITC experiments with wtDnaK, however, higher concentrations were used (0.27−0.67 mg/mL), and therefore small amounts of dimer or higher order wtDnaK species that might be present would influence the binding stoichiometry value by decreasing it, as we observed. In this regard, it is interesting that the DnaK(2−517) species does not show any deviation from the expected 1:1 interaction. The deviation from a 1:1 Langmuir interaction in the case of the SPR experiments is manifested by double-exponential sensorgrams. Inspecting the residuals for the single-exponential fits (Figure 4C), we see that only early time points, prior to achieving equilibrium, deviate from the single-exponential function (which indicates the presence of a rapid initial step). In contrast, the equilibrium end point of

each sensorgram is well fitted by the single-exponential function. The ITC experiments probed the equilibrium end points. The K_d values obtained from the two techniques are identical within experimental error (Table 1).

We suggest that GrpE binds to ligand-free wtDnaK more rapidly than previously thought: specifically, that GrpE·wtDnaK complex formation occurs with a second-order rate constant equal to $(3.4 \pm 0.6) \times 10^5$ M^{-1} s^{-1} rather than $(3-5) \times 10^4$ M^{-1} s^{-1} (*14*). Such a rapid on-rate agrees with an HPLC study of GrpE·wtDnaK complex formation (*37*) that showed complex formation occurs with $k_{on} > 1$ s^{-1}. In that study, the wtDnaK (16 μM) concentration was larger than the concentration of GrpE. Using our on-rate constant, and the value 16 μM, the calculated rate of GrpE·wtDnaK complex formation is 5.4 s^{-1} ($=3.4 \times 10^5$ M^{-1} $s^{-1} \times 16 \times 10^{-6}$ M).

Truncation of the Lid. This study showed that truncating DnaK's lid (residues 518−638) results in complex formation kinetics in accord with a 1:1 Langmuir model, that K_d decreases from ~80 to 4 nM, and that the enhanced affinity is related, in part, to a slower off-rate [$(3.3 \pm 1.6) \times 10^{-2}$ s^{-1} (wt) → $(1.2 \pm 1.2) \times 10^{-3}$ s^{-1} (517)] (Figure 5, Table 1). The combined experiments indicate that GrpE·DnaK(2−517) complexes dissociate more slowly than GrpE·wtDnaK complexes because GrpE's 33-residue flexible, N-terminal tail is bound in the substrate-binding pocket [see GrpE(1−33) Binds in the Substrate-Binding Pocket of DnaK below].

If deletion of DnaK's lid permits easier access of GrpE's tail into the substrate-binding site of DnaK and this binding increases the affinity of the interaction, then deletion of GrpE residues 1−33 should weaken the interaction between GrpE and DnaK. This is exactly what we found: The K_d for the interaction between DnaK(2−517) and GrpE(34−197) increases to 21 nM [compared to 4.5 nM for the interaction between DnaK(2−517) and GrpE] (Table 1). Notice, however, that this K_d is still less than observed for the interaction between wtDnaK and GrpE (64−97 nM). This result reinforces our conclusion that residues 1−33 of GrpE bind into the substrate-binding pocket of DnaK(2−517), and this enhances the affinity of the interaction (compared to the wild-type protein). On the other hand, the enhanced affinity of DnaK(2−517) to GrpE is probably not due entirely to the binding of GrpE's flexible tail into the substrate-binding pocket of DnaK.

From our size exclusion chromatography experiments, we know that the wild-type protein elutes with a larger than expected mass, whereas the lidless variant, DnaK(2−517), elutes with the expected mass. Thus, a distinct possibility is that truncating DnaK's lid (residues 518−638) alters the conformation of the β-sandwich domain or the ATPase domain or both, and the altered conformation binds with enhanced affinity to GrpE.

ATP Induces a Conformational Change in DnaK(2−388). Investigation of complex formation between GrpE and the ATPase domain of DnaK (DnaK388) revealed two novel findings. (i) It is well-known that no detectable GrpE·wtDnaK complex formation occurs in the presence of ATP (*38*). This is because ATP binding induces a global conformational change in wtDnaK (*39*, *40*), and this ATP-bound conformation does not bind to GrpE. We showed here, for the first time, that ATP also prevents the formation of GrpE·DnaK(2−388) complexes (Figure 6). ATP binding must, therefore, induce a conformational change in DnaK(2−388) that abolishes GrpE binding. (ii) Unencumbered by the substrate-binding and lid domains, DnaK(2−388) binds to GrpE with a quite large on-rate constant ($k_{on} = 1.3 \times 10^6$ M^{-1} s^{-1}). Recall that the on-rate constant for GrpE binding to wtDnaK and DnaK(2−517) is identical within the experimental error ($k_{on} \approx 3 \times 10^5$ M^{-1} s^{-1}) (Table 1). These results show that the substrate-binding domain of DnaK retards the rate of GrpE·DnaK complex formation. Possibly, the substrate-binding domain masks a surface of the ATPase domain that is required for rapid binding to GrpE.

Interaction between GrpE and the Substrate-Binding Domain of DnaK. This is the first study to show that the substrate-binding domain of DnaK, residues 393−507, reversibly binds to GrpE. That DnaK(393−507) does not bind to GrpE(34−197) shows that residues 1−33 are necessary for GrpE·DnaK(393−507) complex formation. One possibility is that the flexible tail region of GrpE binds directly into the substrate-binding pocket of DnaK. In this sense, GrpE residues 1−33 may be thought of as a competitive inhibitor of substrate (poly)peptides. Notice that GrpE residues 1−33, MSSKEQKTPEGQAPEEIIMDQHEEIEAVEPEAS, are a highly negatively charged segment of protein. Given that DnaK has a propensity to bind positively charged peptides that contain a hydrophobic core (*41*) and that negative charges, particularly located within the peptide, inhibit binding, it is indeed remarkable that the GrpE tail binds to DnaK at all. On the other hand, the on- and off-rate constants for the interaction of GrpE's tail with the substrate-binding domain of DnaK are similar to the on- and off-rate constants for the Cro peptide (MQERITLKDYAM), which also contains internal negatively charged residues. In detail, the k_{on} and k_{off} values for GrpE·DnaK(393−507) complex formation are 100 M^{-1} s^{-1} and 0.0067 s^{-1} (Table 1), respectively, whereas the k_{on} and k_{off} values for wtDnaK·Cro complex formation are 18 M^{-1} s^{-1} and 0.00013 s^{-1} (*22*), respectively.

At this time, however, we cannot eliminate the possibility that the flexible region of GrpE, residues 1−33, binds *outside* the substrate-binding pocket of DnaK(393−507). A peptide bound in either trans [DnaK(393−507)·p5] or cis [DnaK(386−562)] could alter the conformation of the β-sandwich domain in such a way as to eliminate the GrpE binding site or weaken the interaction. NMR experiments have documented that peptide binding indeed alters the conformation of the loops and strands that make up the β-sandwich domain, which is the key structural feature of DnaK(393−507) (*26*). That GrpE's flexible tail accelerates peptide dissociation from preformed DnaK−peptide complexes (*16*, *17*) suggests that GrpE's flexible tail is not just a competitive inhibitor (of the substrates that bind in the pocket). Either GrpE's flexible tail probably binds outside the pocket (and this binding catalyzes the release of the bound substrate) or GrpE's tail binds inside the substrate-binding pocket at a site not occupied by the bound substrate [and this binding catalyzes a peptide exchange reaction, in that Grp(1−33) displaces the bound (poly)peptide substrate]. Given the numerous hints that DnaK possesses two sites for substrate (poly)peptide (*27*, *42*, *43*), the possibility that GrpE's tail binds outside the substrate-binding pocket is reasonable. It is noteworthy that certain cationic peptides have been shown to catalyze the release of bound antigenic peptides from preformed class

Table 2: Comparison of Kinetic and Thermodynamic Constants for the Reactions between BAG-1 and Nucleotide-Free Hsc70(1−540) and between GrpE and Nucleotide-Free DnaK(2−517)

binding partners	k_{on} (M^{-1} s^{-1})	k_{off} (s^{-1})	K_d (nM)	ΔH (kcal/mol)
BAG-1 + Hsc70(1−540)[a]	5.3×10^5	2.7×10^{-1}	100 (ITC) 500 (SPR)	−12.5
GrpE + DnaK(2−517)	2.7×10^5	1.2×10^{-3}	3.5 (ITC) 4.5 (SPR)	−12.9

[a] Data taken from ref *46*.

II MHC−peptide complexes (*44*, *45*). This chemistry is analogous to the action of GrpE's tail on substrate release from preformed DnaK−substrate complexes.

Presently, we do not know the significance of the interaction between the flexible tail of GrpE and DnaK. We know that the tail residues are not needed for DnaK-mediated protein folding, because DnaK/DnaJ/GrpE(34−197) mediates the refolding of unfolded luciferase (*14*). On the other hand, on the basis of sequence analysis of several GrpE orthologues, a flexible domain of approximately 33 residues appears to be present in all GrpE proteins, although the specific sequences are not conserved. Obviously, other experiments are needed to uncover the biological relevance of GrpE's tail.

Comparison to BAG-1−Hsc70 Interactions. It is interesting to compare our results to those reported for the interaction between BAG-1, a eukaryotic nucleotide exchange factor, and a nucleotide-free, lidless form of human Hsc70 (540-residue fragment) (*46*). BAG-1 is a monomer in solution and is structurally distinct from GrpE in that it contains neither the long paired, N-terminal coiled-coil domain nor the 33-residue flexible domain (residues 1−33). Despite the structural differences, GrpE and BAG-1 interact with the same subdomains on their respective ATPase domains (*47*). The parameters for the reaction between GrpE and DnaK(2−517) and between BAG-1 and Hsc70(1−540) are given in Table 2. Two of the parameters (k_{on} and ΔH) are remarkably similar. The primary difference is the affinity of the respective interactions: K_d for the BAG-1·Hsc70(1−540) interaction falls in the range 100−500 nM, whereas K_d for the GrpE·DnaK(2−517) interaction equals ∼4 nM. Most of the difference between the two K_d values is due to the different k_{off} values [0.267 s^{-1} (BAG-1) versus 1.2×10^{-3} s^{-1} (GrpE)]. Our interpretation is that GrpE interacts with DnaK at many more sites than BAG-1 interacts with Hsc70, and this greater number of interaction sites between GrpE and DnaK significantly slows down complex dissociation (compared to BAG-1 and Hsc70).

To summarize, we have shown that GrpE·wtDnaK complex formation is faster than previously thought; deletion of DnaK's lid (residues 518−638) results in a significant enhancement in the affinity of the GrpE·DnaK interaction; via its flexible tail, GrpE binds to the substrate-binding domain of DnaK; and ATP binding induces a conformational change in DnaK(2−388) that prevents complex formation with GrpE. To achieve a complete understanding of the interaction between DnaK and GrpE, it will be necessary in the future to determine how interdomain coupling in DnaK affects GrpE binding and how ADP modulates the kinetics of GrpE·DnaK complex formation.

ACKNOWLEDGMENT

We thank Dr. Donard Dwyer for preparing the figure containing structures.

REFERENCES

1. Bukau, B., and Horwich, A. L. (1998) *Cell 92*, 351−366.
2. Ellis, R. J., and Hartl, F. U. (1999) *Curr. Opin. Struct. Biol. 9*, 102−110.
3. Hartl, F. U., and Hayer-Hartl, M. (2002) *Science 295*, 1852−1858.
4. Slepenkov, S. V., and Witt, S. N. (2002) *Mol. Microbiol. 45*, 1197−1206.
5. Packschies, L., Theyssen, H., Bucherberger, A., Bukau, B., Goody, R. S., and Reinstein, J. (1997) *Biochemistry 36*, 3417−3422.
6. Laloraya, S., Gambill, B. D., and Craig, E. A. (1994) *Proc. Natl. Acad. Sci. U.S.A. 91*, 6481−6485.
7. Naylor, D. J., Hoogenraad, N. J., and Hoj, P. B. (1996) *FEBS Lett. 396*, 181−188.
8. Stines, A. P., Naylor, D. J., Hoj, P. B., and van Heeswijck, R. (1999) *Plant Physiol. 120*, 923.
9. Naylor, D. J., Stines, A. P., Hoogenraad, N. J., and Hoj, P. B. (1998) *J. Biol. Chem. 273*, 21169−21177.
10. Padidam, M., Reddy, V. S., Beachy, R. N., and Fauquet, C. M. (1999) *Plant Mol. Biol. 39*, 871−881.
11. Kabani, M., Beckerich, J. M., and Brodsky, J. L. (2002) *Mol. Cell. Biol. 22*, 4677−4689.
12. Schönfeld, H.-J., Schmidt, D., Schröder, H., and Bukau, B. (1995) *J. Biol. Chem. 270*, 2183−2189.
13. Wu, B., Wawrzynow, Zylicz, M., and Georgopoulos, C. (1996) *EMBO J. 15*, 4806−4816.
14. Harrison, C. J., Hayer-Hartl, M., Di Liberto, M., Hartl, F.-U., and Kuriyan, J. (1997) *Science 276*, 431−435.
15. Jordan, R., and McMacken, R. (1995) *J. Biol. Chem. 270*, 4563−4569.
16. Mally, A., and Witt, S. N. (2001) *Nat. Struct. Biol. 8*, 254−257.
17. Mehl, A. F., Heskett, L. D., and Neal, K. M. (2001) *Biochem. Biophys. Res. Commun. 282*, 562−569.
18. Grimshaw, J. P., Jelesarov, I., Schonfeld, H. J., and Christen, P. (2001) *J. Biol. Chem. 276*, 6098−6104.
19. Groemping, Y., and Reinstein, J. (2001) *J. Mol. Biol. 314*, 167−178.
20. Groemping, Y., Klostermeier, D., Herrmann, C., Veit, T., Seidel, R., and Reinstein, J. (2001) *J. Mol. Biol. 305*, 1173−1183.
21. Gelinas, A. D., Langsetmo, K., Toth, J., Bethoney, K. A., Stafford, W. F., and Harrison, C. J. (2002) *J. Mol. Biol. 323*, 131−142.
22. Farr, C. D., Galiano, F. J., and Witt, S. N. (1995) *Biochemistry 34*, 15574−15582.
23. Slepenkov, S. V., and Witt, S. N. (1998) *Biochemistry 37*, 1015−1024.
24. Gao, B., Greene, L., and Eisenberg, E. (1994) *Biochemistry 33*, 2048−2054.
25. Bukau, B., and Walker, G. C. (1989) *J. Bacteriol. 171*, 6030−6038.
26. Pellecchia, M., Montgomery, D. L., Stevens, S. Y., Vander Kooi, C. W., Feng, H.-P., Gierasch, L. M., and Zuiderweg, E. R. P. (2000) *Nat. Struct. Biol. 7*, 298−303.
27. Wang, H., Kurochkin, A. V., Pang, Y., Hu, W., Flynn, G. C., and Zuiderweg, E. R. P. (1998) *Biochemistry 37*, 7929−7940.
28. Wiseman, T., Williston, S., Brandts, J. F., and Lin, L. N. (1989) *Anal. Biochem. 179*, 131−137.
29. Bevington, P. R. (1969) *Data Reduction and Error Analysis for the Physical Sciences*, McGraw-Hill, New York.
30. Montgomery, D., Jordan, R., McMacken, R., and Freire, E. (1993) *J. Mol. Biol. 232*, 680−692.
31. Flaherty, K. M., DeLuca-Flaherty, C., and McKay, D. B. (1990) *Nature 346*, 623−628.
32. Slepenkov, S. V., and Witt, S. N. (2002) *Biochemistry 41*, 12224−12235.
33. Mayer, M. P., Laufen, T., Paal, K., McCarty, J. S., and Bukau, B. (1999) *J. Mol. Biol. 289*, 1131−1144.
34. Buchberger, A., Schroder, H., Buttner, M., Valencia, A., and Bukau, B. (1994) *Nat. Struct. Biol. 1*, 95−101.
35. Morton, T. A., and Myszka, D. G. (1998) *Methods Enzymol. 295*, 268−294.
36. Slepenkov, S. V., Patchen, B., Peterson, K. M., and Witt, S. N. (2003) *Biochemistry 42*, 5867−5876.

37. Reid, K. L., and Fink, A. L. (1996) *Cell Stress Chaperones 1*, 127−137.
38. Zylicz, M., Ang, D., and Georgopoulos, C. (1987) *J. Biol. Chem. 262*, 17437−17442.
39. Palleros, D. R., Reid, K. L., Shi, L., Welch, W. J., and Fink, A. L. (1993) *Nature 365*, 664−666.
40. Schmid, D., Baici, A., Gehring, H., and Christen, P. (1994) *Science 263*, 971−973.
41. Gragerov, A., Zeng, L., Zhao, X., Burkholder, W., and Gottesman, M. E. (1994) *J. Mol. Biol. 235*, 848−854.
42. Farr, C. D., and Witt, S. N. (1997) *Biochemistry 36*, 10793−10800.
43. Koller, M. F., Baici, A., Huber, M., and Christen, P. (2002) *FEBS Lett. 520*, 25−29.
44. Pedrazzini, T., Sette, A., Albertson, M., and Grey, H. M. (1991) *J. Immunol. 146*, 3496−3501.
45. DeKroon, A. I. P. M., and McConnell, H. M. (1993) *Proc. Natl. Acad. Sci. U.S.A. 90*, 8797−8801.
46. Stuart, J. K., Myszka, D. G., Joss, L., Mitchell, R. S., McDonald, S. M., Xie, Z., Takayama, S., Reed, J. C., and Ely, K. R. (1998) *J. Biol. Chem. 273*, 22506−22514.
47. Sondermann, H., Scheufler, C., Schneider, C., Hohfeld, J., Hartl, F. U., and Moarefi, I. (2001) *Science 291*, 1553−1557.
48. Zhu, X., Zhao, X., Burkholder, W. F., Gragerov, A., Ogata, C. M., Gottesman, M. E., and Hendrickson, W. A. (1996) *Science 272*, 1606−1614.
49. Laemmli, U. K. (1970) *Nature 227*, 680−685.

BI0346493